

Journal of Mechanics of Materials and Structures

**STRESS-MINIMIZING HOLES WITH A GIVEN SURFACE ROUGHNESS
IN A REMOTELY LOADED ELASTIC PLANE**

Shmuel Vigdergauz and Isaac Elishakoff

Volume 15, No. 1

January 2020



STRESS-MINIMIZING HOLES WITH A GIVEN SURFACE ROUGHNESS IN A REMOTELY LOADED ELASTIC PLANE

SHMUEL VIGDERGAUZ AND ISAAC ELISHAKOFF

We proposed a new form of modeling the boundary roughness effects on the stress distribution and stress concentration around a single hole in a loaded thin elastic plate. The shape irregularities are simulated as periodic patterns of notch-like deviations from an “ideal” shape (mostly from a circle). These are assessed with two relative measures: their maximum peak-to-valley height and the average slope. At given hole shape, all expressions for stress fields are derived in explicit form. This analysis serves as a basis to formulate and numerically solve the optimization problem of finding the stress-minimizing hole shape under fixed irregularities levels. In doing so, the surface topography need not be shallow as was supposed in previous studies.

Methodologically, this study continues the previous work of the authors in detecting the “worst” hole shape under certain extremizing conditions [Vigdergauz and Elishakoff 2019]. The performance of the proposed scheme is verified via instructive numerical examples. The results obtained are presented graphically and may be analyzed visually. They have a practical relevance for optimal design problems in mechanical engineering.

1. Introduction

The problem of determining stress distributions and reducing the stress concentration factor (SCF) around holes in thin flat elastic plates occurs in numerous design situations. The SCF is defined here as the (dimensionless) ratio between the maximum hoop stress and unit applied stresses.

Stress concentrations are highly localized effects which are functions of loading mode and geometry. At given shape, the direct problem of finding SCF is solved, analytically or numerically, for a host of different cases together spanning a large range of possibilities as summarized, for instance, in [Pilkey and Pilkey 2007]. In addition to the SCF, a modern physical explanation of the influence of local shape irregularities on fatigue and fracture mechanical performance also includes the volumetric strain energy density approach (see, for instance, [Pluvinage 2003; Savruk and Kazberuk 2017]) which is beyond our scope.

The paper is focused on nonideal hole-shapes with technologically inevitable irregularities. These are well approximated by isolated notches which can be described by several geometric parameters: the notch peak-to-valley height ρ , the notch edge angle ϑ and the notch radius [Pluvinage 2003]. The latter is less important in the current context of the shape-smoothing SCF minimization, while the first two are chosen here as lower constraints on the shape roughness under which the SCF-minimizing hole is found numerically through a global optimization approach.

Vigdergauz is the corresponding author.

Keywords: 2D-elastostatic problem, Kolosov–Muskhelishvili potentials, shape optimization, stress concentration factor, shape irregularity, genetic algorithm.

This research, therefore, has three key novel aspects. First, we introduce easy-to-measure geometrical parameters well applicable separately or in combination to quantitatively assess the shapes irregularities. Second, together with the primary analytical findings from [Vigdergauz 2006; Vigdergauz and Elishakoff 2019], these are embedded into a stable and fast GA-based optimization scheme which can be handled by modern computers. Third, its efficient numerical implementation permits to identify the SCF-minimizing hole shape in an elastic plate over a wide variety of the governing parameters. Especially interesting here is the notch edge slope ϑ which has not received sufficient attention in the literature so far.

The findings of this study are in line with the earlier conducted studies [Vigdergauz and Cherkaev 1986; Cherkaev et al. 1998; Vigdergauz 2006; Vigdergauz and Elishakoff 2019].

The remainder of this paper is organized as follows: for reader's convenience, Section 2 summarizes the complex valued direct solver of the considered 2D model; Section 3 introduces and describes in detail the suggested geometrical constraints; in these terms the precise problem formulation is presented in Section 4; and then Section 5 gives the solution scheme and some computational hints for practical applications; Section 6 displays representative numerical examples to illustrate the use of the proposed approach and demonstrate its effectiveness and rationality. Concluding remarks are offered in Section 7.

2. Basic model: assumptions and notations

This whole section contains mainly classical material. We choose to include it nevertheless, since the novel parts of this works to be presented in the next sections, will refer to many of the equations in this section.

2.1. Problem setup. Consider Figure 1. Let a thin infinite linear elastic plate be weakened by a hole with a p -fold rotationally symmetric boundary L_p enclosing the origin of the plane E of a complex variable $z = x + iy \in E$. Suppose further that the plate is remotely loaded by uniform nontangential stresses

$$\sigma_{xx}^\infty = P, \quad \sigma_{yy}^\infty = Q, \quad \sigma_{xy}^\infty = 0, \quad (2-1)$$

while the hole is traction-free:

$$\sigma_{nn}(t), \sigma_{n\tau}(t) \equiv 0, \quad t \in L_p; \quad (2-2)$$

where $\sigma(t) = \{\sigma_{nn}, \sigma_{\tau\tau}, \sigma_{n\tau}\}$ denotes the stress tensor in a local system of curvilinear orthogonal coordinates (n, τ) at a point $t \in L_p$.

Let also the infinite material-filled domain S outside the hole be conformally mapped onto the exterior T of the unit circle γ in the auxiliary complex ζ -plane by the holomorphic function $\omega(\zeta)$, $\zeta \in T$ which has only finite number M of the Laurent terms:

$$L_p : t = \omega(\xi), \quad t \in L_p; \quad \xi = \exp(i\phi) \in \gamma, \quad |\xi| = 1; \quad \omega(\zeta) = \zeta + \sum_{m=1}^M \frac{d_m}{\zeta^{pm-1}}, \quad |\zeta| \geq 1. \quad (2-3)$$

By the required mapping uniqueness the coefficients $\{d_m\}$ are necessarily bounded by the successfully narrowing intervals [Ahlfors 1953]

$$-\frac{1}{\sqrt{pm-1}} \leq d_m \leq \frac{1}{\sqrt{pm-1}}; \quad m = 1, 2, \dots, M. \quad (2-4)$$

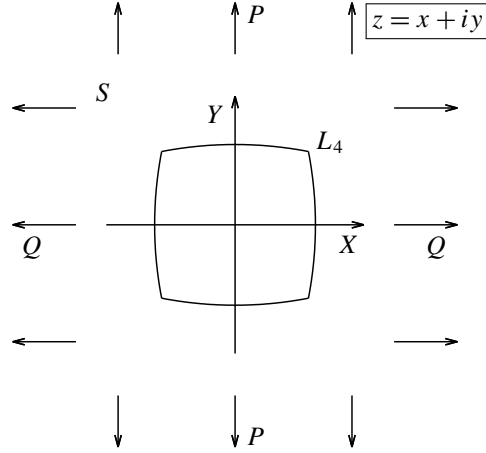


Figure 1. The problem schematic: an infinite plate with a traction-free hole under uniform stresses, the cases $P = Q$ and $P = -Q$ correspond to remote bulk and shear, respectively. The piecewise smooth hole boundary possesses a certain p -fold rotational symmetry as exemplified here for $p = 4$.

For $M = 1$, the equal sign in (2-4) defines (up to rigid rotation) the limiting case of a p -cusped hypocycloid identified in the optimization context in [Givoli and Elishakoff 1992; Shahzad et al. 2017; Vigdergauz and Elishakoff 2019].

Equation (2-3) provides, in effect, a finite parametrization of an arbitrary closed curve $L_p = L_p(d_1, d_2, \dots, M)$, which is approximated as a point in an M -dimensional rectangular parallelepiped Π_M with the edges of the length (2-4). This is further used as a searching space to find the globally optimal hole shape (Section 4) with taking $\{d_m\}$ as the design variables. In view of the loading symmetry (2-1) they can be taken as real-valued quantities without loss of generality.

The integers $p = 2, 3, 4, \dots$ and $M = 1, 2, 3, \dots$ are governing parameters determining the behavior of the numerical simulations and their convergence to a stable solution (Section 6).

2.2. Kolosov–Muskhelishvili formalism for 2D linear elasticity. This widely known approach replaces the biharmonic real-valued Airy function with two complex-valued functions $\Phi_0(\zeta)$, $\Psi_0(\zeta)$, $\zeta \in T$ [Muskhelishvili 1963] commonly referred to as the KM potentials. They are analytic functions in T and continuously extendible on γ . The loading conditions (2-1), (2-2) are then equivalently expressed as

$$\Phi_0(\zeta) = B + \Phi(\zeta); \quad \Psi_0(\zeta) = \Gamma + \Psi(\zeta), \quad \zeta \in \Sigma; \quad \Phi(\zeta), \Psi(\zeta) = O(|\zeta|^{-2}); \quad (2-5a)$$

$$4B = \text{Tr}\{\sigma^\infty\} = Q + P; \quad 2\Gamma = \text{Dev}\{\sigma^\infty\} = Q - P; \quad \text{Im } B, \text{Im } \Gamma = 0; \quad (2-5b)$$

and

$$-\frac{2}{\xi^2} \overline{\omega'(\xi)} [\text{Re } \Phi(\xi) + B] + \overline{\omega(\xi)} \Phi'(\xi) + \Gamma \omega'(\xi) = -\omega'(\xi) \Psi(\xi), \quad \xi \in \gamma; \quad (2-6)$$

respectively. The terms in (2-6) are rearranged specifically for later use [Kalandiya 1975].

At any given shape L_p , identities (2-5), (2-6) comprise together the direct boundary-value problem in $\Phi(\xi)$, $\Psi(\xi)$. This formulation allows to employ the rich machinery of the complex-variable theory.

Especially relevant here is to expand the KM potentials in the convergent Laurent series (the summation begins with $k = 2$ to match the asymptotic (2-5a))

$$\Phi(\zeta) = \sum_{k=2}^{\infty} a_k \zeta^{-k}, \quad \Psi(\zeta) = \sum_{k=2}^{\infty} b_k \zeta^{-k}, \quad \zeta \in \Sigma + \gamma. \quad (2-7)$$

The coefficients $\{a_k\}$, $\{b_k\}$ may partially vanish due to the adopted rotational symmetry. Nevertheless, one should keep in mind that both expansions are *infinite* even for a *finite*-term mapping $\omega(\zeta)$ [Muskhelishvili 1963].

2.3. Explicit closed form of the hoop stress. The left-hand side of (2-6) is the boundary value of an T -holomorphic function tending to zero at infinity. In turn, this means that its series expansion involves no nonnegative powers in ζ . Substitution of (2-3) and (2-7) in (2-6) with zeroing the resultant coefficients for ζ^n , $n \geq 0$ gives the infinite linear algebraic system in a_k , $k \geq 2$ [Kalandiya 1975]

$$a_{j+2} - \sum_{k=1}^j (j-k+1) \bar{d}_{j-k+1} a_k - (j+1) \sum_{k=1}^{\infty} \bar{d}_{j+k+1} \bar{a}_k = A_j, \quad j = 0, 1, \dots, \quad (2-8a)$$

$$A_0 = 2B - \Gamma, \quad A_1 = 0, \quad A_j = -2B(j+1) \bar{d}_{j+1}, \quad j \geq 2. \quad (2-8b)$$

The first sum is omitted in (2-8a) when $j = 0, 1$. Again, by the symmetry arguments, the above equations may be eliminated partially from the system, thus facilitating the computations.

Actually, the second potential $\Psi(\zeta)$ remains outside the system thus allowing to separate out the coefficients $\{a_k\}$ only needed to compute the boundary hoop stress $\sigma_{\tau\tau}(\xi)$ [Muskhelishvili 1963]

$$\sigma_{\tau\tau}(\xi) = 4 \operatorname{Re} \Phi_0(\xi) \quad (2-9)$$

that are of our interest here. Note in passing that by the principle of maximum applied to harmonic function $\operatorname{Re} \Phi_0(\zeta)$ we have for the hoop stress average over an arbitrary hole shape (at $|P|, |Q| = 1$, for definiteness)

$$\overline{\sigma_{\tau\tau}} = \Phi_0(\infty) = 2 \implies K = \max |\sigma_{\tau\tau}(\xi)| \geq 2, \quad (2-10)$$

where K stands for the SCF.

Remarkably, for the finite term mapping (2-3) system (2-8) breaks up into two subsystems

- (a) the first M nonvanishing equations for the first M unknowns $\{a_k\}$ and
- (b) the infinite remainder for the “tail” $\{a_k\}$, $k > M$.

The key feature of the subsystem (b)enumi is its finite-differences structure [Levy and Lessman 1958] by which the “tail” is expressed *analytically* through the first M unknowns as proved at length in [Vigdergauz 2006; Vigdergauz and Elishakoff 2019]. The resultant formula reads

$$\Phi_0(\xi) = B + \frac{R_M(\bar{\xi})}{\xi \omega'(\bar{\xi})}, \quad (2-11)$$

where $R_M(\xi)$ is a polynomial of degree M in ξ :

$$R_M(\xi) = r_M \xi^M + r_{M-1} \xi^{M-1} + \dots + r_0 \quad (2-12)$$

with the coefficients

$$r_0 = a_1 = 0, \quad r_1 = a_2, \quad r_m = a_{m+1} - \sum_{k=2}^m (-1)^k k d_k a_{m+k+1}, \quad m \geq 2. \quad (2-13)$$

In other words, equations (2-11)–(2-13) are *exact* up to negligible errors caused by numerically solving the subsystem (a)enumi at moderate values of M . When, for example, $p = 4$, the numerical simulations gives stable results at most for $M = 8 \div 12$.

Note that just this (almost) analytical solution of the direct problem provides the numerical effectiveness of the SCF local optimization.

3. Geometrical constraints

The question here is how to quantitatively assess the deviations of real holes surfaces $R(\theta)$ from the nominally “ideal” shape with no local disturbances or spikes, like, say, a circle ($R(\theta) = \text{constant}$). We advance the following two easy-to-measure dimensionless factors:

(1) The maximum peak-to-valley normalized height,

$$\rho[L_p] = \frac{R_{\max} - R_{\min}}{R_{\max}}, \quad 0 \leq \rho \leq 1, \quad R_{\max} = \max R(\theta), \quad R_{\min} = \min R(\theta), \quad \theta \in \lambda_p, \quad (3-1)$$

which equals to zero only for a circle. Here $\lambda_p = [0; \pi/p]$ is the irreducible angular interval along L_p . Any given $\rho > 0$ corresponds to a variety of curves from an ellipse with eccentricity $\sqrt{\rho(2-\rho)}$ to a highly irregular shape with many notches around the perimeter as exemplified in Section 6 (Figure 8, left).

(2) The normalized variation of $R(\theta)$

$$V[L_p] = \frac{\text{var}[L_p]}{R_{\max}} \geq 0. \quad (3-2)$$

In conformity with the theory of real-valued functions [Natanson 1955], the (bounded) variation $\text{var}[L_p]$ is here defined through the nonnegative discrete sums of absolute values of the differences of the radii between each two adjacent points on the irreducible part L

$$\text{var}[L_p] = \sup \sum_{i=0}^n |R(\arg(\theta_{i+1})) - R(\arg(\theta_i))| \geq 0, \quad \{t_i\} \in L, \quad \{\arg(t_i)\} \in \lambda_p. \quad (3-3)$$

The supremum is taken over all possible partitions of L_p with an arbitrary set of points t_0, t_1, \dots, t_n ordered by a chosen direction of traversing. Clearly, only one such set is used in numerically evaluating the variations.

The variations are nontrivially bounded below [Natanson 1955] as

$$\text{var}[L_p] \geq R_{\max} - R_{\min}, \quad (3-4)$$

where the equal sign is true for only monotonic functions so that

$$V[L_p] \geq \rho[L_p]. \quad (3-5)$$

Say, the shape shown in the above-mentioned Figure 8 (left) has a small ratio $\rho = 0.019$ and a markedly larger variation $V = 2\rho = 0.038$ by which the function $R(\theta)$ is forced to oscillate along the hole perimeter.

For a differentiable function $R(\theta)$ one has with (3-2)

$$V[L_\rho] = R_{\max}^{-1} \int_0^{\pi/p} |R'(\theta)| d\theta. \quad (3-6)$$

Again, as before, $V[L_\rho]$ is zero only on a circle $R(\theta) = \text{constant}$.

Remark. For an arbitrary one-term mapping (2-3) $\omega(\zeta) = \zeta + d_m \zeta^{1-pm}$ both parameters take the same value thus reaching the equal sign in (3-5). Indeed, in view of (3-6),

$$R^2(\theta) = 1 + 2d_m \cos p\theta + d_m^2; \quad (3-7a)$$

$$R_{\max} = 1 + |d_m| \quad \text{and} \quad R_{\min} = 1 - |d_m|, \quad \text{therefore} \quad \rho = \frac{2|d_m|}{1 + |d_m|}; \quad (3-7b)$$

$$V[L_\rho] = \frac{2pd_m}{1 + |d_m|} \int_0^{\pi/p} \frac{|\sin p\theta|}{\sqrt{1 + 2d_m \cos p\theta + d_m^2}} d\theta = \frac{2|d_m|}{1 + |d_m|} = \rho[L_\rho]. \quad (3-7c)$$

With (3-4) the last identity is however evident: function $R(\theta)$ is monotonic in each irreducible part of L_ρ since $\text{sgn}(R'(\theta)) = -\text{sgn}(d_n)$, $\theta \in \lambda_p$.

Generally speaking, ρ and V are not interrelated for $M > 1$. On the contrary, they basically complement each other in that ρ defines the maximal relative height of the notches while V is, through (3-6), proportional to the tangent of the average slope angle $\bar{\vartheta}$ of the notches edges. These are precisely the parameters used in [Palmov 1963; Sheinin 1972] in developing a probabilistic risk evaluation of the surface roughness, thus possibly bridging the gap between deterministic and stochastic uncertainty assessments. In the current optimization context, their interplay becomes all the more intimate (Section 6) returning us again to the equal sign in (3-5).

Before leaving this section we note the following useful features of the proposed approach:

- Neglecting the V -factor may adversely affect the accuracy of some previous published results [Medina and Hinderliter 2014; Chang et al. 2017] where the restriction of very small slopes $\vartheta \ll 1$ was involved. Taking into account irregularities tilts substantially expands the practicability of this study.
- Mathematically, an integral-type assessment V of the slopes provides a numerically stable optimization scheme and requires less computational efforts than direct angular differentiation of $R(\vartheta)$ between closely spaced points.
- Both parameters do not need to be as small as frequently supposed in the literature.

4. One-side constraining inequalities and problem statement

Our aim is to numerically minimize the SCF at given ρ and V in a representative interval of their values. For embedding these constraints into the minimization framework it is desirable to reformulate them as one-side inequalities. For this purpose we recall the previous result in [Vigdergauz 2006], which states that the unconstrained K -minimizing shape is always a circle with one exception of the four-fold

symmetric hole under remote shear. In this case (named S_4 for brevity) the optimal shape looks as a smoothed quadrangle with

$$\rho^* = V^* = 0.23, \quad K = 2.78, \quad (4-1)$$

in contrast to the circle-related value $K = 4$. Keeping this in mind, we intuitively conjecture that here the SCF is a monotonically decreasing function of either of these two quantities from zero to ρ^* and an increasing one afterward while in all other cases it increases monotonically everywhere. Then one can introduce the following constraining inequalities:

$$\rho \leq \rho_0, \quad \rho_0 \in [0, \rho^*], \quad \rho \geq \rho_0, \quad \rho_0 \geq \rho^*, \quad S_4 \text{ case}; \quad (4-2a)$$

$$\rho \geq \rho_0, \quad \rho_0 \geq 0, \quad \text{any other case}; \quad (4-2b)$$

and analogously for V . These are tailored especially to fix *a priori* the intervals of monotonicity of the functions $K(\rho)$, $K(V)$. Both ρ - and V -types can be applied either separately or together. For the case (4-2b) they are used directly while for (4-2a), their appropriate combination is given and explained in Section 6.

It is hoped that the adequate choice of the inequality sign within each interval will make the $K(\rho)$ minimum occur exactly at the boundary point ρ_0 . This presumption is fully justified by the numerical simulations for a set of ρ^* and V values in the representative interval $[0, 0.75]$ (Section 6).

Remark. Noteworthy is that the SCF-minimizing ρ and V values coincide not only for S_4 as indicated by (4-1) but also for the general minimization case as revealed by the numerical simulations.

With these preliminaries we are now in a position to quantitatively formulate the following optimization problem:

Given an external loading type to find, over all admissible set of the design variables $\{d_m\}$, the p -symmetrical hole shape $L_p \in \Pi_M$ which minimizes the stress concentration factor K under either or both (ρ and V) constraint types (4-2)

$$K(L_p, M, c^*) \xrightarrow{\{d_m\}} \min(p, M, c^*). \quad (4-3)$$

Here c^* abstractly denotes given thresholds ρ^* , V^* .

5. Numerical solution procedure

Computationally, (4-3) is a rather standard optimization problem whose numerical solution is conveniently obtained by an iterative loop over successively modified shapes with computing the criterion K (fitness function) of each candidate. For this purpose, we apply the approach developed and validated in the first author's previous paper [Vigdergauz 2006]. It includes three main ingredients: an enhanced direct solver (2-11)–(2-13), a standard GA-based global searching engine (see, for instance, [Goldberg and Sastry 2007]) and an efficient shape encoding scheme (2-3) within the GA framework. The use of a global scheme rather than a gradient-type scheme is intended to avoid being trapped by the highly nonlinear and sensitive cost function K .

The GA starts with randomly generating an initial population of individual binary strings that might be possible solutions. Each string concatenates M randomly generated two-byte signed integers I_m :

$-W \leq I_m \leq W$, $W = 2^{15} - 1$, $m = \overline{1, M}$. In view of (2-4), this encodes a shape L_p within the searching space Π_M as

$$d_m = \frac{I_m}{W\sqrt{m}}, \quad m = 1, 2, \dots, M. \quad (5-1)$$

Substitution of (5-1) into (2-3) decodes the corresponding shape. However, in doing so, self-intersecting shapes may appear, since the inequalities (2-4) are only necessary, but not sufficient to guarantee their absence. To the author's best knowledge, no conditions imposed on the Laurent terms (2-3) to effectively trim out any self-intersection are known thus far. Therefore, we check each decoded curve for possibly breaking the monotonicity

$$\frac{d \arg \omega(\theta)}{d\theta} \geq 0, \quad \theta \in \lambda_p, \quad (5-2)$$

which provides the more restrictive shape property of star-shapedness. It is clear, physically, that only star-shaped holes are promising for optimization. In the numerical simulations (Section 6) this is attested to by the fact that the optimal values of $\{d_m\}$ are rather distant from the intervals limiting values (2-4).

After decoding each string into the corresponding shape its fitness K is then computed through (2-11)–(2-13) at a large number of the unit circle points. Whenever the current shape violates any imposed constraint, including (5-2), a significant constant penalty is assigned as its fitness value without further computation of K . After that, all strings are subject to the GA binary operations of 1-point crossover and mutations performed with certain predefined probability levels to obtain offspring.

This is repeated many times (typically several hundreds) up to achieving a stable solution which is believed to be close to the global optimum.

The stopping criterion is a problematic issue in GA iterations as there are no practical means to assess the actual error in real applications. Instead, the optimization is stopped after some N_{iter} iterations — in belief that the process really converges. However, at specific stochastic combinations, GAs may become “stuck” quite far from the global optimum. This is prevented by multiple GA runs carried out for every result point. Practically, N_{iter} is chosen in such a way that the optimization criterion remains unchanged in successive iterations well in advance of termination. For the problem at hand, we averaged five runs per point with $N_{\text{iter}} = 200 \div 500$ depending on specific values of the governing parameters.

6. Numerical results

This constrained optimization scheme is tested numerically in the most informative case of square symmetry ($p = 4$) except for the case $p = 64$ in Section 6.3. For comparison convenience, the results obtained are displayed and commented (wherever possible) in parallel for both bulk and shear loading modes. They are further grouped into three subsections according to constraints combinations preimposed on the shape geometry.

6.1. The ρ -inequality constraint alone. Our first set of computations is carried out with no V -constraint when the minimization problem (4-3) is treated only under ρ -inequalities (4-2). The resultant curves in Figure 2 visualize the attainable lower bound on $K(\rho)$ as yielded by the GA searching.

The corresponding K -minimizing hole shapes (normalized to the unit area) are exemplified in Figure 3. Here the attention is drawn to the resultant smoothly shaped “arms”, which are gradually lengthening in an attempt to match the growing constraint ρ . Notice that in the shear (antisymmetric) mode the

GA optimizes also the shapes orientation by aligning the “arms” along the diagonals $y = \pm x$ where the (continuous) hoop stress $\sigma_{\tau\tau}(\theta)$ must change its sign. This is of no concern in the isotropic bulk mode but we rotate them through the same angle for easier comparison to their shear-related counterparts.

Figure 4 illustrates the shape convergence to the stable solution with increasing number M of the mapping terms at a given ρ . One can see that the bulk mode exhibits faster convergence ($M \geq 8$ against $M \geq 12$). This can directly be attributed to the higher local curvature occurring near the diagonal since this is the only substantial difference between the shapes.

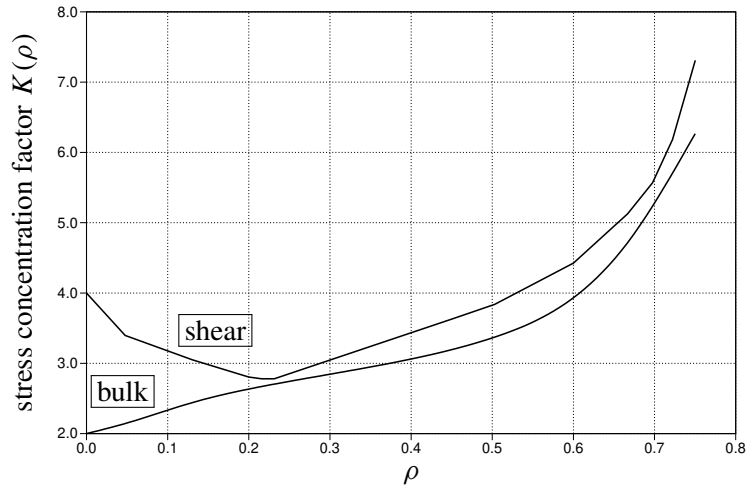


Figure 2. The minimal attainable $K(\rho)$ for the basic loads.

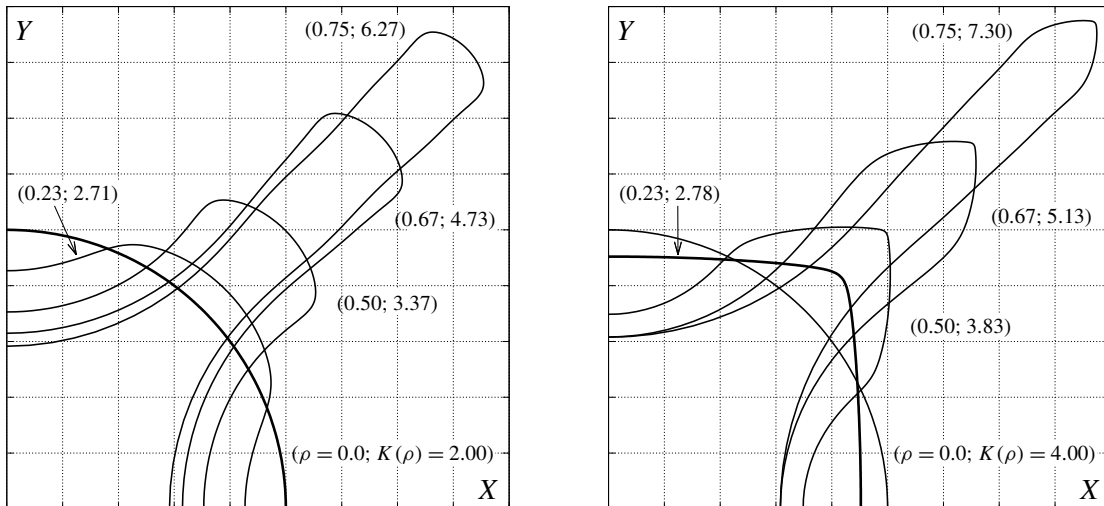


Figure 3. The upper-right quarter of K -optimal hole: the shape evolution with increasing ρ for bulk load (left) and pure shear (right). The globally optimal shapes at $\rho = 0.0$ and $\rho = 0.23$, respectively (Equation (4-1)), are emboldened for better comparison.

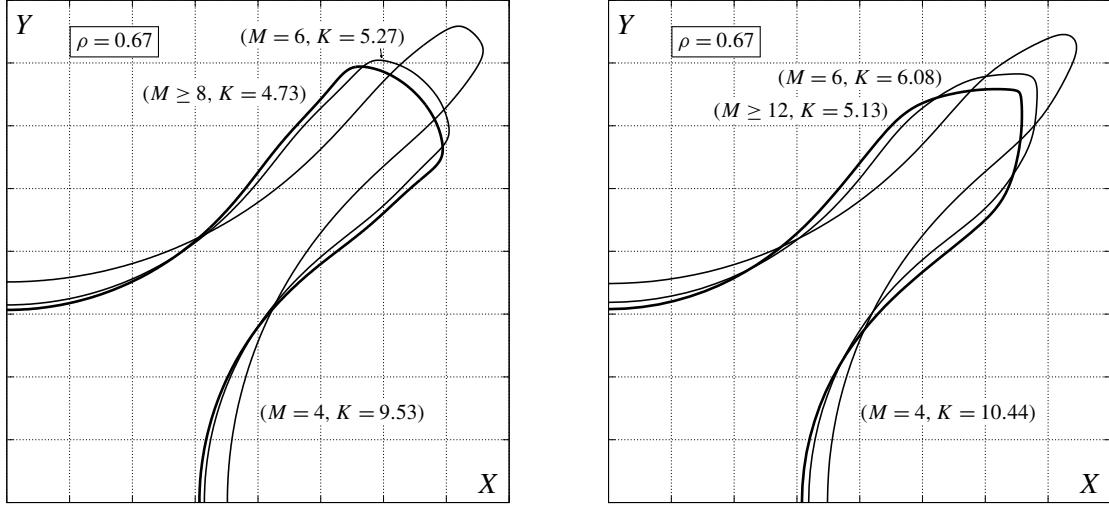


Figure 4. The upper-right quarter of K -optimal hole: the shape convergence to the stable state (bolded lines) at $\rho = 0.67$ with increasing number M of nonzero mapping terms for bulk load (left) and pure shear (right).

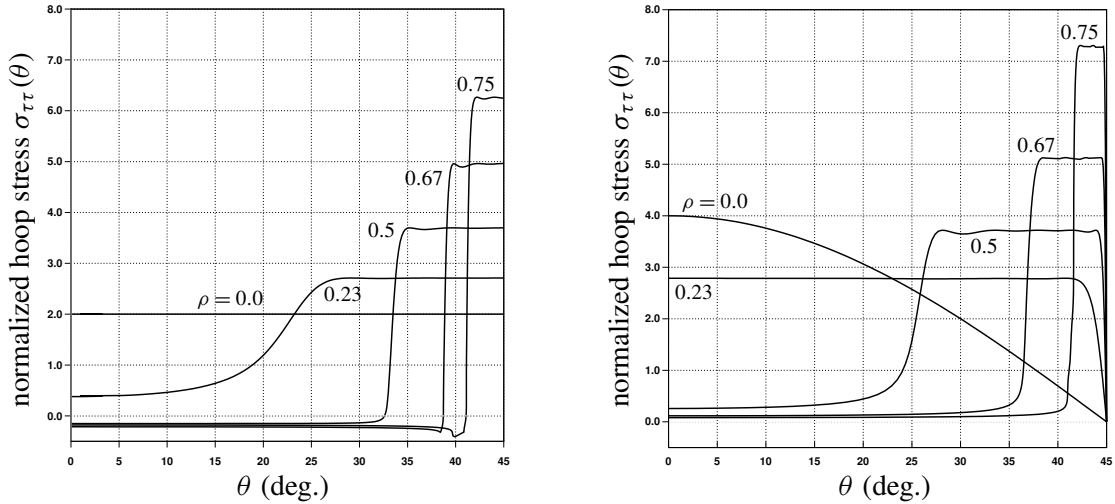


Figure 5. The upper-right quarter of K -optimal hole: the hoop stress angular distribution in the physical plane E for bulk load (left) and pure shear (right).

The angular stress distributions $\sigma_{\tau\tau}(\theta)$ (normalized by the unit load) along the K -minimal shapes in the physical plane E is depicted by Figure 5. Interestingly, with the increasing ρ , the distributions form a distinct step near the diagonal while remaining almost zero along the rest of the shape. To avoid confusion, note that the bulk-related nonzero stress average (2-10) holds only in the auxiliary ζ -plane as shown in explanatory Figure 6.

Such piecewise constant pattern is consistent with two others obtained previously in the similar context:

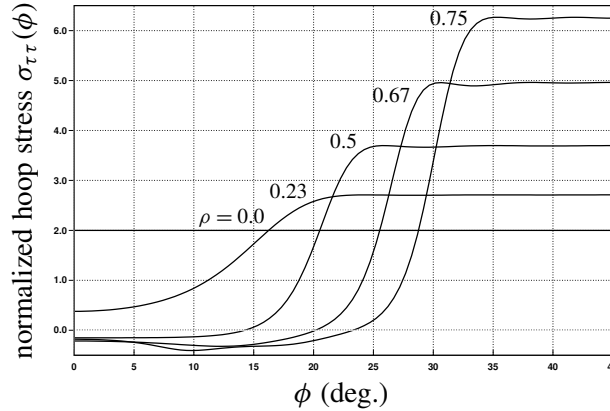


Figure 6. The bulk case: the hoop stress from the left-side of Figure 4 depicted along the unit circle γ in the auxiliary complex plane.

- (a) the unrestricted minimization of K under pure shear [Vigdergauz 2006];
- (b) the stress-smoothing optimization in perforated checkerboard structures [Vigdergauz 2012].

This numerically found smoothing-minimization relationship should be studied also analytically in the future. This is more so relevant since combination of the equistress concept advanced in [Cherepanov 1974] and the maximum principle [Ahlfors 1953] for harmonic function $\Phi(z)$ proves directly that both criteria are equivalent at least for the unconstrained shape optimization of several holes under bulk-dominating remote load [Vigdergauz 1976].

Figure 7 presents a typical dependence of the K -minimum stress distribution on the number of held mapping terms. As this shows, the stress peak and attendant oscillations are progressively being smoothed by larger M .

We see, therefore, that the bulk- and shear-related K -minimum hole shapes have exactly the same *integral* measures ρ and V but differ *locally* as clearly seen in Figure 3.

Finally, of special importance is that *a posteriori* computed normalized variation $V(\rho)$ of the K -minimum shapes appear, in numerical fact, to attain the smallest possible values everywhere for $\rho \in [0, 0.75]$ by saturating the nonzero lower bound for monotonous functions (3-5): $V(\rho) = V_{\min}(\rho) = \rho$. To put it differently, the ρ -constrained minimization of the SCF has the nice property of minimizing the optimal shape variation as well:

$$K_{\rho}^{(0)} \equiv \min K(\rho_0) \leftrightarrow V_{\min}(\rho_0) \equiv V_{\rho}^{(0)} = \rho_0, \quad (6-1)$$

endowing the function $R(\theta)$ with the monotonicity property in the irreducible interval λ_p . However, the exact explanation of this remains unclear.

6.2. The V -inequality constraint alone. Here, the limitations are obtained from (4-2) by the evident substitution of ρ , ρ_0 , ρ^* with V , V_0 , V^* , respectively. With the established monotonicity of the functions $\min K(\rho)$ and $V_{\min}(\rho)$, one can write analogously to (6-1),

$$K_V^{(0)} \equiv \min K(V_0) \leftrightarrow \min \rho(V_0) \equiv \rho_V^{(0)} = V_0, \quad (6-2)$$

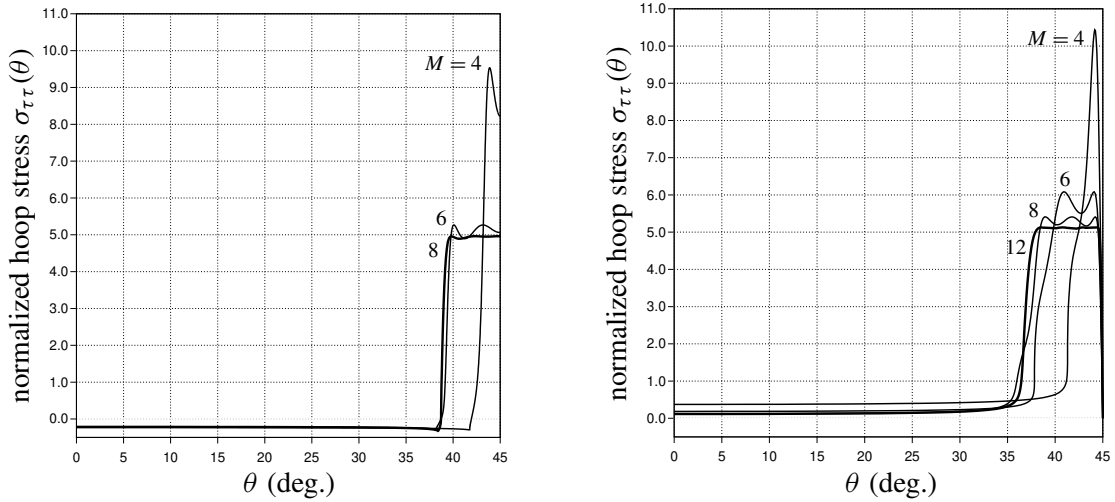


Figure 7. The upper-right quarter of K -optimal hole: hoop stress convergence to the stable state (bolded lines) at $\rho = 0.67$ with increasing number M of nonzero mapping terms for bulk load (left) and pure shear (right).

so that if $K_V^{(0)} = K_\rho^{(0)}$ then $\rho_V^{(0)} = \rho_0$, $V_\rho^{(0)} = V_0$. Therefore, taken separately, both ρ - and V -constraints return the same optimal results already detailed in the previous subsection, as expected.

6.3. Both constraints combined. Taken together, they have a nontrivial sense only as the following inequality constraints

$$\rho \leq \rho_0, \quad V \geq V_0, \quad V_0 > \rho_0, \quad (6-3)$$

where the last one is introduced to conform with the general relation (3-5). The evident modification of (6-3) for the exceptional S_4 case is omitted here to save space.

The first two opposite-sided bounds are intended to detect the K -minimizing shapes with $V > \rho$ (and hence with $K(V) > K(\rho)$) which appear to be unattainable by applying these constraints separately as before. The stronger this inequality is and the larger p is, the more wavy is the K -optimal hole shape with increasing number of smoothed notches as exemplified in Figure 8 (left). Again, as before, the resultant optimal shapes tend to avoid the hoop stress jumps or singularities with a step-like pattern of the tangential stresses (Figure 8, right). The oscillations observed along the step's top side are caused by the local nature of the K -minimum criterion. These are small (with the valley-to-peak ratio greater than 96.5%) and may be further diminished with increasing M . More extended numerical results are too bulky to be presented here. We will analyze this case in the future.

7. Concluding remarks

We advanced two possible parameters with clear engineering meaning for geometrically measuring hole-shape irregularities. These are maximum height and average steepness of the shape deviations easily embedded into the stable and highly accurate numerical scheme of the constrained minimization of the stress concentration factor. The results obtained give a good indication of the SCF attainable lower limit

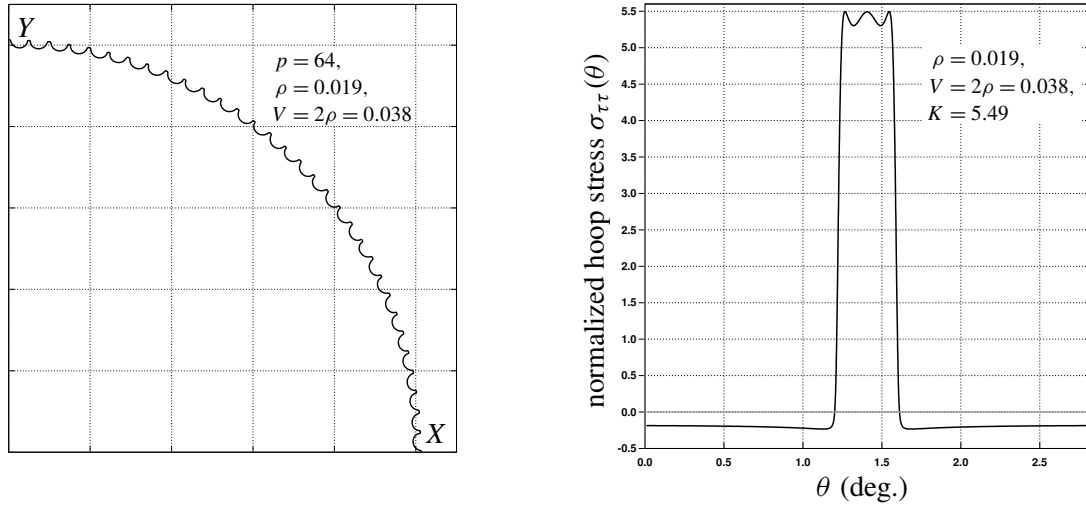


Figure 8. Both constraints together for bulk load and $p = 64$: the upper-right quarter of K -optimal hole (left) and the corresponding hoop stress (right) at $V > \rho$.

and the corresponding hole shapes. Fascinatingly, the K -minimum hoop stress distributions tend to be piecewise constant with a distinctive step along strongly rounded notches and a very small stress value and gradient in all other locations.

It should be emphasized that the analytical direct solver ((2-11)–(2-13)) cannot be extended to the next in complexity cases of a single elastic inclusion or several interacting holes. Here, new approaches are required for a stable and accurate minimization of the local K -criterion.

References

- [Ahlfors 1953] L. V. Ahlfors, *Complex analysis: an introduction to the theory of analytic functions of one complex variable*, McGraw-Hill, New York, 1953.
- [Chang et al. 2017] Z. Chang, R. Liao, and W. Lu, “Surface stress concentration factor via Fourier representation and its application for machined surfaces”, *Int. J. Solids Struct.* **113-114** (2017), 108–117.
- [Cherepanov 1974] G. P. Cherepanov, “Inverse problems of the plane theory of elasticity”, *Prikl. Mat. Mekh.* **38:6** (1974), 963–979. In Russian; translated in *J. Appl. Math. Mech.* **38:6** (1974) 915–931.
- [Cherkaev et al. 1998] A. V. Cherkaev, Y. Grabovsky, A. B. Movchan, and S. K. Serkov, “The cavity of the optimal shape under the shear stresses”, *Int. J. Solids Struct.* **35:33** (1998), 4391–4410.
- [Givoli and Elishakoff 1992] D. Givoli and I. Elishakoff, “Stress concentration at a nearly circular hole with uncertain irregularities”, *J. Appl. Mech.* **59:25** (1992), S65–S71.
- [Goldberg and Sastry 2007] D. E. Goldberg and K. Sastry, *Genetic algorithms: the design of innovation*, 2nd ed., Springer, 2007.
- [Kalandiya 1975] A. I. Kalandiya, *Mathematical methods of two-dimensional elasticity*, Mir, Moscow, 1975.
- [Levy and Lessman 1958] H. Levy and F. Lessman, *Finite difference equations*, Pitman, London, 1958.
- [Medina and Hinderliter 2014] H. Medina and B. Hinderliter, “The stress concentration factor for slightly roughened random surfaces: analytical solution”, *Int. J. Solids Struct.* **51:10** (2014), 2012–2018.
- [Muskhelishvili 1963] N. I. Muskhelishvili, *Some basic problems of the mathematical theory of elasticity*, Noordhoff, Groningen, Netherlands, 1963.

- [Natanson 1955] I. P. Natanson, *Theory of functions of a real variable*, Ungar, New York, 1955.
- [Palmov 1963] V. A. Palmov, “State of stress in the neighborhood of a rough surface of elastic bodies”, *Prikl. Mat. Mekh.* **27**:5 (1963), 963–969. In Russian; translated in *J. Appl. Math. Mech.* **27**:5 (1963), 1479–1489.
- [Pilkey and Pilkey 2007] W. D. Pilkey and D. F. Pilkey, *Peterson’s stress concentration factors*, 3rd ed., Wiley, New York, 2007.
- [Pluvinage 2003] G. Pluvinage, *Fracture and fatigue emanating from stress concentrators*, Springer, 2003.
- [Savruk and Kazberuk 2017] M. P. Savruk and A. Kazberuk, *Stress concentration at notches*, Springer, 2017.
- [Shahzad et al. 2017] S. Shahzad, F. Dal Corso, and D. Bigoni, “Hypocycloidal inclusions in nonuniform out-of-plane elasticity: stress singularity vs. stress reduction”, *J. Elasticity* **126**:2 (2017), 215–229.
- [Sheinin 1972] V. I. Sheinin, “On the asymptotic method for calculating stress near rough surface of elastic solids”, *Izv. Akad. Nauk SSSR Mekh. Tverd. Tela* **2** (1972), 94–102. In Russian; translated in *Mech. Solids* **7**:2 (1972), 94–102.
- [Vigdergauz 1976] S. B. Vigdergauz, “Integral equation of the inverse problem of the plane theory of elasticity”, *Prikl. Mat. Mekh.* **40** (1976), 566–569. In Russian; translated in *J. Appl. Math. Mech.* **40**:3 (1976), 518–522.
- [Vigdergauz 2006] S. Vigdergauz, “The stress-minimizing hole in an elastic plate under remote shear”, *J. Mech. Mater. Struct.* **1**:2 (2006), 387–406.
- [Vigdergauz 2012] S. Vigdergauz, “Stress-smoothing holes in an elastic plate: from the square lattice to the checkerboard”, *Math. Mech. Solids* **17**:3 (2012), 289–299.
- [Vigdergauz and Cherkaev 1986] S. B. Vigdergauz and A. V. Cherkaev, “A hole in a plate, optimal for its biaxial extension-compression”, *Prikl. Mat. Mekh.* **50**:3 (1986), 524–528. In Russian; translated in *J. Appl. Math. Mech.* **50**:3 (1986), 401–404.
- [Vigdergauz and Elishakoff 2019] S. Vigdergauz and I. Elishakoff, “Energy-maximizing holes in an elastic plate under remote loading”, *J. Mech. Mater. Struct.* **14**:1 (2019), 139–154.

Received 28 Jun 2019. Revised 27 Aug 2019. Accepted 28 Sep 2019.

SHMUEL VIGDERGAUZ: shmuelvigdergauz@gmail.com
R&D Division, The Israel Electric Corp. Ltd., Haifa, Israel

ISAAC ELISHAKOFF: elishako@fau.edu
Department of Mechanical Engineering, Florida Atlantic University, Boca Raton, FL, United States

JOURNAL OF MECHANICS OF MATERIALS AND STRUCTURES

msp.org/jomms

Founded by Charles R. Steele and Marie-Louise Steele

EDITORIAL BOARD

ADAIR R. AGUIAR	University of São Paulo at São Carlos, Brazil
KATIA BERTOLDI	Harvard University, USA
DAVIDE BIGONI	University of Trento, Italy
MAENGHYO CHO	Seoul National University, Korea
HUILING DUAN	Beijing University
YIBIN FU	Keele University, UK
IWONA JASIUKEWICZ	University of Illinois at Urbana-Champaign, USA
DENNIS KOCHMANN	ETH Zurich
MITSUTOSHI KURODA	Yamagata University, Japan
CHEE W. LIM	City University of Hong Kong
ZISHUN LIU	Xi'an Jiaotong University, China
THOMAS J. PENCE	Michigan State University, USA
GIANNI ROYER-CARFAGNI	Università degli studi di Parma, Italy
DAVID STEIGMANN	University of California at Berkeley, USA
PAUL STEINMANN	Friedrich-Alexander-Universität Erlangen-Nürnberg, Germany
KENJIRO TERADA	Tohoku University, Japan

ADVISORY BOARD

J. P. CARTER	University of Sydney, Australia
D. H. HODGES	Georgia Institute of Technology, USA
J. HUTCHINSON	Harvard University, USA
D. PAMPLONA	Universidade Católica do Rio de Janeiro, Brazil
M. B. RUBIN	Technion, Haifa, Israel

PRODUCTION production@msp.org

SILVIO LEVY Scientific Editor

Cover photo: Ev Shafir

See msp.org/jomms for submission guidelines.

JoMMS (ISSN 1559-3959) at Mathematical Sciences Publishers, 798 Evans Hall #6840, c/o University of California, Berkeley, CA 94720-3840, is published in 10 issues a year. The subscription price for 2020 is US \$660/year for the electronic version, and \$830/year (+\$60, if shipping outside the US) for print and electronic. Subscriptions, requests for back issues, and changes of address should be sent to MSP.

JoMMS peer-review and production is managed by EditFLOW® from Mathematical Sciences Publishers.

PUBLISHED BY

 **mathematical sciences publishers**
nonprofit scientific publishing

<http://msp.org/>

© 2020 Mathematical Sciences Publishers

Journal of Mechanics of Materials and Structures

Volume 15, No. 1

January 2020

Stress-minimizing holes with a given surface roughness in a remotely loaded elastic plane	SHMUEL VIGDERGAUZ and ISAAC ELISHAKOFF	1
Analytical modeling and computational analysis on topological properties of 1-D phononic crystals in elastic media	MUHAMMAD and C. W. LIM	15
Dynamics and stability analysis of an axially moving beam in axial flow	YAN HAO, HULIANG DAI, NI QIAO, KUN ZHOU and LIN WANG	37
An approximate formula of first peak frequency of ellipticity of Rayleigh surface waves in an orthotropic layered half-space model	TRUONG THI THUY DUNG, TRAN THANH TUAN, PHAM CHI VINH and GIANG KIEN TRUNG	61
Effect of number of crowns on the crush resistance in open-cell stent design	GIDEON PRAVEEN KUMAR, KEPING ZUO, LI BUAY KOH, CHI WEI ONG, YUCHENG ZHONG, HWA LIANG LEO, PEI HO and FANGSEN CUI	75
A dielectric breakdown model for an interface crack in a piezoelectric bimaterial	YURI LAPUSTA, ALLA SHEVELEVA, FRÉDÉRIC CHAPELLE and VOLODYMYR LOBODA	87
Thermal buckling and free vibration of Timoshenko FG nanobeams based on the higher-order nonlocal strain gradient theory	GORAN JANEVSKI, IVAN PAVLOVIĆ and NIKOLA DESPENIĆ	107
A new analytical approach for solving equations of elasto-hydrodynamics in quasicrystals	VALERY YAKHNO	135
Expansion-contraction behavior of a pressurized porohyperelastic spherical shell due to fluid redistribution in the structure wall	VAHID ZAMANI and THOMAS J. PENCE	159



1559-3959(2020)15:1;1-L